Cum Laude Poster Award

MR Coil Sensitivity Inhomogeneity Correction for Plaque Characterization in Carotid Arteries

Olivier Salvado[a], Claudia Hillenbrand[b], Jasjit Suri[a], David Wilson[a];
[a] Dept. of Biomedical Enginering, Case Western Reserve University, Cleveland, OH 44106;
[b] Dept. of Radiology , University Hospitals of Cleveland, Cleveland, OH 44106.

ABSTRACT

We are involved in a comprehensive program to characterize atherosclerotic disease using multiple MR images having different contrast mechanisms (T1W, T2W, PDW, magnetization transfer, etc.) of human carotid and animal model arteries. We use specially designed intravascular and surface array coils that give high signal-to-noise but suffer from sensitivity inhomogeneity. With carotid surface coils, challenges include: (1) a steep bias field with an 80% change; (2) presence of nearby muscular structures lacking high frequency information to distinguish bias from anatomical features; (3) many confounding zero-valued voxels subject to fat suppression, blood flow cancellation, or air, which are not subject to coil sensitivity; and (4) substantial noise. Bias was corrected using a modification of the adaptive fuzzy c-mean method reported by Pham et al. (IEEE TMI, 18:738-752), whereby a bias field modeled as a mechanical membrane was iteratively improved until cluster means no longer changed. Because our images were noisy, we added a noise reduction filtering step between iterations and used ≈ 5 classes. In a digital phantom having a bias field measured from our MR system, variations across an area comparable to a carotid artery were reduced from 50% to <5% with processing. Human carotid images were qualitatively improved and large regions of skeletal muscle were relatively flat. Other commonly applied techniques failed to segment the images or introduced strong edge artifacts. Current evaluations include comparisons to bias as measured by a body coil in human MR images.

Keywords: Atherosclerosis, carotid, MRI, bias field, inhomogeneity, classification, segmentation, fuzzy C-means.

1. INTRODUCTION

Magnetic resonance imaging (MRI) can be used to diagnose and stage blood vessel disease by identifying lumen narrowing in a stenosis, by measuring blood flow, and by imaging plaque in the arterial wall[1]. We are focusing on the latter application in a comprehensive program that includes new imaging technologies such as intravascular coils, high field MRI, imaging agents, and advanced computer image analysis. Several studies have shown the pertinence of using MR imaging to characterize atherosclerosis lesions *in vivo*[2;3]. There is good evidence that experts can identify and quantify plaque components such as lipid and fibrous tissue using multiple MR images having different contrast mechanisms[1;4]. Our goal is to create robust, accurate computer algorithms to perform this tissue typing.

Here, we report a method for bias correction that will automatically correct the signal intensities in carotid artery images. The principal degradation is the spatial inhomogeneity of coil sensitivity of the specially designed surface coils. A correction algorithm faces many challenges. First, the receive coils suffer from a very steep sensitivity fall-off in the direction of increasing depth that is much more significant than the variation across the brain when imaging with a head coil. If not well corrected, this can confound the examination of the vessel wall by experts and defeat automatic tissue classification algorithms. Second, the noise present in the MRI carotid images can disrupt algorithms. Third, there are many voxels close to the artery walls that are void of signal, from either the fat suppression or blood flow compensation. Fourth, there are relatively large skeletal muscle areas in the neck, near the carotid arteries, that do not include sufficient high spatial frequency content to separate the variations of the sensitivity inhomogeneity from the anatomical structures. Common methods of bias field correction, mainly developed for brain imaging[5], fail in the face of these challenges.

Medical Imaging 2004: Image Processing, edited by
J. Michael Fitzpatrick, Milan Sonka, Proceedings of SPIE Vol. 5370
(SPIE, Bellingham, WA, 2004) · 1605-7422/04/$15 · doi: 10.1117/12.535958

We report a bias correction algorithm to address these challenges consisting of a modified, adaptive fuzzy c-mean method with a mechanical membrane model of the bias field [6]. We first describe the algorithm and the many special modifications required for carotid artery images including noise reduction filtering, background segmentation, outlier class identification, and signal normalization. We then describe various phantom evaluations and application to patient data.

2. METHOD

Early methods for correcting the sensitivity inhomogeneity present in MR images assumed that the frequencies of the ideal image and the frequencies of the bias field do not overlap. They rely on linear filtering and induce edge artifacts. We are interested in the artery wall and we use blood flow suppression as well as fat suppression techniques. The area we want to analyze is thus surrounded by voxels void of signal (lumen and surrounding fat), making edge artifacts prominent with one of these techniques.

Other methods assume that the ideal image is corrupted by a multiplicative bias field with slow spatial variations. Algorithms have been proposed to estimate this bias field by optimizing the histogram of the corrected image, either by modeling it with clustering[6;7] techniques or by entropy minimization [8]. To insure a smooth bias field one can use low order polynomial function[9;10], surface B-splines[11], or a bias field with many degrees of freedom but with smoothing constraints[6]. The carotid artery images are acquired with two phased array coils with two coils each, placed on either side of the neck. The sensitivity variations of the final reconstructed image using the sum-of-square algorithm present overlap of the sensitivity of the four coils that cannot be well approximated with a low order polynomial. We opted for a bias field without support, constrained only by an energy functional mimicking elastic and thin plate behavior.

In order to optimize the bias field we assumed further that the underlying image is made of a small number of different tissues and is piece-wise constant across the neck. Our algorithm assumes a finite number of tissue classes and optimizes the bias field by minimizing a fuzzy C-means energy cost function following earlier work [6]. We chose this approach after observing that the neck images consist of many relatively large areas of skeletal muscles, bones and connective tissues. Other common methods include entropy minimization of the histogram or maximization of posterior probabilities. The former is sensible to noise and requires a large number of voxels to be statistically significant, while the latter increases the computation burden for similar performance to the C-means algorithm. The fuzzy C-Means algorithm is also sensitive to noise, and since our images can include a significant amount of noise, we perform a pre-processing filtering step.

The observed MRI signal Y is the product of the true signal X generated by the underlying anatomy and the spatially varying field B, and additive noise, N. At voxel j in the image domain Ω:

$$y_j = x_j b_j + n_j \quad ; j \in \Omega \tag{1}$$

2.1. Noise filtering

We use region growing with seeds at the top corners to identify the voxels outside the neck. From these regions in air, we estimate the additive noise mean (μ_n) and standard deviation (σ_n), to give a background class in the classification step [12]. This background class will not contribute to bias field estimation since it is void of signal and therefore not subject to the RF coil sensitivity.

Black et al. [13] proposed a version of anisotropic diffusion filtering with a diffusion coefficient based on the Tukey's biweight functional (3). The image is subject to a diffusion process perpendicular to the gradient when it is lower than σ_{AD} and is unchanged otherwise. We used the estimated noise variance from the background voxels to obtain the parameter σ_{AD}. Assuming that the noise, n, is stationary, Gaussian, and independent with standard deviation σ_n, then ∇x is also normally distributed with zero mean and standard deviation $\sigma_n\sqrt{2}$. We use this value as an estimate for the filter parameter $\sigma_{AD} = \sigma_n\sqrt{2}$ in a conservative way and $\sigma_{AD} = 2\sigma_n\sqrt{2}$ as an upper limit. We set the number of iterations of the anisotropic diffusion filtering to nine voxels by analogy to linear Gaussian filtering [14] with a kernel size equal to the slice thickness.

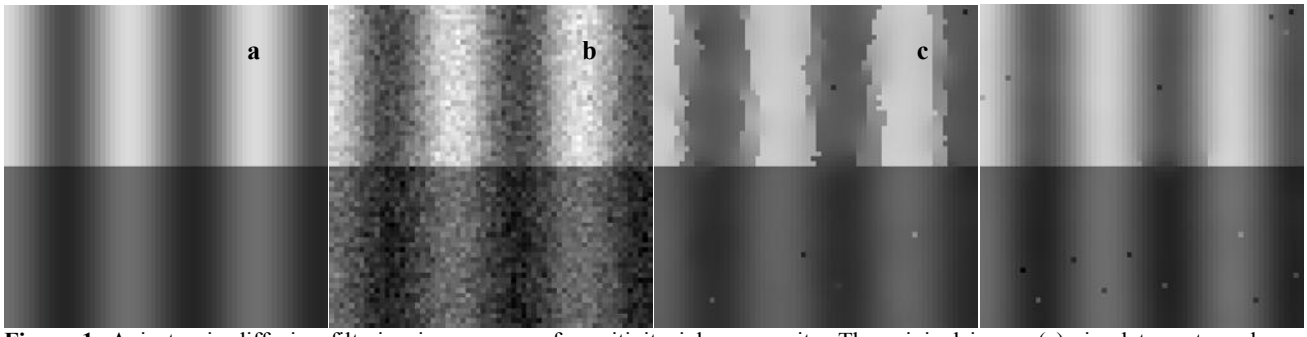

Figure 1: Anisotropic diffusion filtering in presence of sensitivity inhomogeneity. The original image (a) simulates a two-class image with a multiplicative sinusoidal bias field. Additive normal noise is added (b). After filtering with anisotropic diffusion step artifacts appear (c). When the bias field is taken into account as in our proposed scheme, the artifacts are much reduced (d). All images are displayed with the same windowing. The exact bias field is assumed to be known exactly in this case to better exemplify the method.

When sensitivity inhomogeneity is present, the gradient of the bias field corrupts the diffusion process. To remedy this problem, the bias is estimated from the original data by fitting a third order 2D polynomial function on the voxels with significant signal (obtained by applying a threshold to remove background). This rough estimate (B_0) is also used to initialize the bias in the AFCM algorithm. The gradient of B_0 is computed and taken into account in the diffusion equation (figure 1). Our final implementation of the anisotropic diffusion filter is:

$$\frac{\partial I}{\partial t} = -\nabla\left(g\left(\left\|\nabla I - \nabla B_0\right\|\right)\left(\nabla I - \nabla B_0\right)\right) \tag{2}$$

$$\text{where } g(x) = \begin{cases} \left[1-(x/\sigma_{AD})^2\right]^2/2 & |x| \le \sigma_{AD} \\ 0 & \text{otherwise} \end{cases} \tag{3}$$

2.2. The FCM algorithm with spatial inhomogeneity

The original fuzzy C-means [15] is modified to take into account the low frequency perturbation of the cluster centers modeled as a slowly varying bias field. The energy functional to be minimized becomes:

$$E_{FCM} = \sum_{j\in\Omega}\sum_{k=1}^{N_c} u_{jk}^p \left\|y_j - b_j v_k\right\|^2 \tag{4}$$

where y is the signal measured, u is the membership function for the voxel j to the class k, N_c is the number of classes, b is the bias field, and v_k is the gray-scale center of cluster k.

The optimal parameters are found by iterating between the closed form solutions of the zero-gradient conditions for u and v as described by Pham and Prince [6]:

$$u_{jk} = \frac{\left\|y_j - b_j v_k\right\|^{-2/(p-1)}}{\sum_{l=1}^{N_c}\left\|y_j - b_j v_l\right\|^{-2/(p-1)}} \tag{5}$$

and

$$v_k = \frac{\sum_{j\in\Omega} u_{jk}^p b_j y_j}{\sum_{j\in\Omega} u_{jk}^p b_j^2} \tag{6}$$

with the constraint

$$\sum_{k=1}^{N_c} u_{jk} = 1 \tag{7}$$

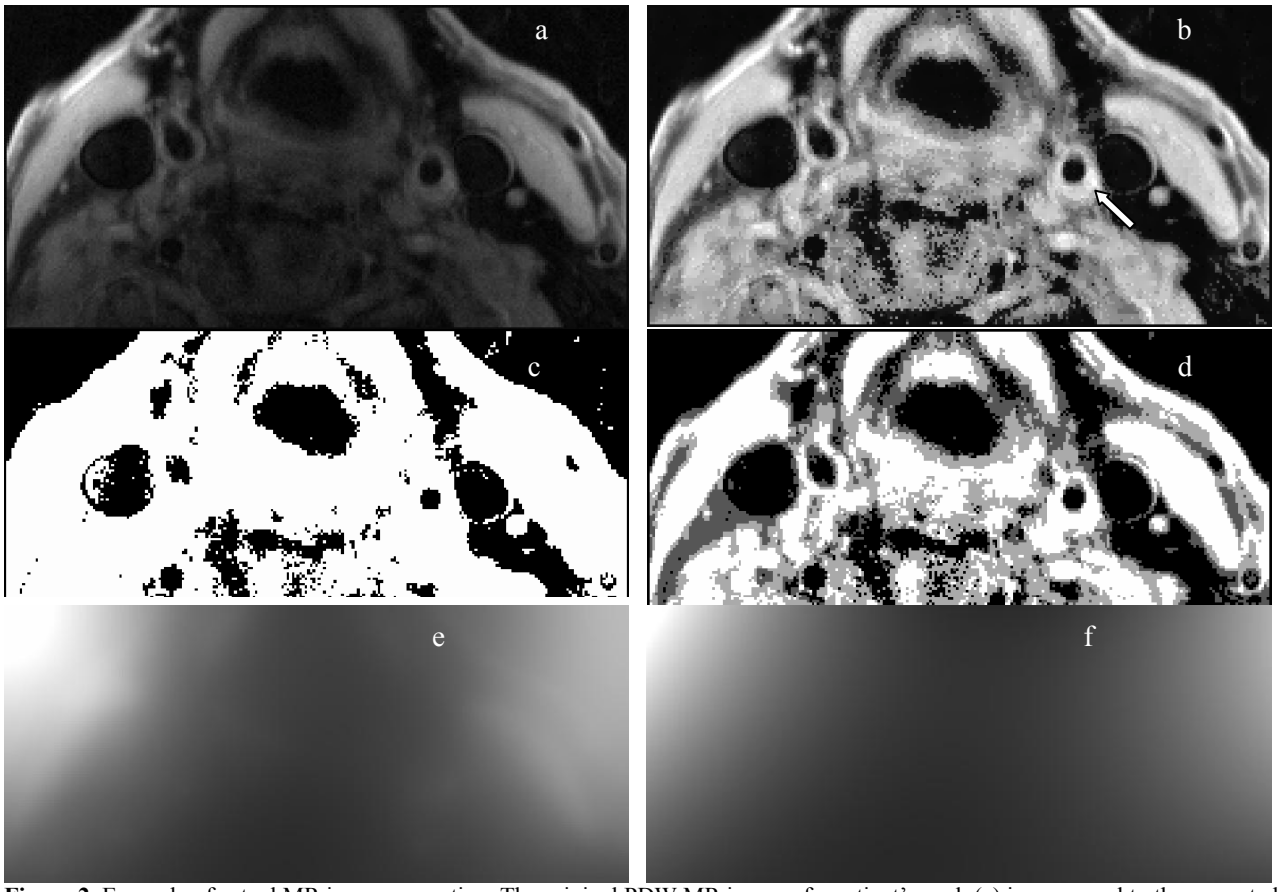

Figure 2. Example of actual MR image correction. The original PDW MR image of a patient's neck (a) is compared to the corrected image (b) where the hyperintense signal in the carotid artery wall (arrow) relative to skeletal muscle is typical of fibrous tissue. The original image is thresholded to segment the voxels with signal (c) using a threshold of ($\mu n+3\sigma n$). The segmented image with 3 tissue classes (d) shows homogeneous values for the muscles across the image. Bottom row shows final bias field estimate (e) and the initial 3rd order polynomial fitting B_0 used for the bias initialization (f).

2.3. Smoothing constraint on the bias

Pham and Prince [6] proposed additional terms to constrain the bias field to be spatially smooth: an elastic membrane (E_{b1}) and a thin plate membrane (E_{b2}) term. The new energy functional to be minimized defines the adaptive fuzzy C-means algorithm (AFCM):

$$E_{AFCM} = \sum_{j\in\Omega}\sum_{k=1}^{N_c} u_{jk}^{p} \left\| y_j - b_j v_k \right\|^2 + \alpha \sum_{j\in\Omega}\sum_{r=1}^{M} (D_r \otimes b)_j^2 + \beta \sum_{j\in\Omega}\sum_{r=1}^{M}\sum_{s=1}^{M} (D_r \otimes D_s \otimes b)_j^2 \tag{8}$$

that we decompose in:

$$E_{AFCM} = E_{FCM} + E_{b1} + E_{b2} \tag{9}$$

They proposed to find b_j by writing the zero-gradient necessary conditions of the energy with respect to b_j and solving the closed-forms resulting equations iteratively as an extra step of the FCM algorithm. The computation of the bias field is computationally intensive and a multigrid approach is presented. We evolve instead the bias field iteratively in the direction of the gradient:

$$\frac{\partial b}{\partial t} = -\left(\nabla E_{FCM} + \nabla E_{b1} + \nabla E_{b2}\right) \tag{10}$$

where:

$$\nabla E_{FCM} = \frac{\partial E_{FCM}}{\partial b_j} = -2\sum_{k=1}^{N_c} u_{jk}^{p} . v_k \left(y_j - b_j v_k\right) \tag{11}$$

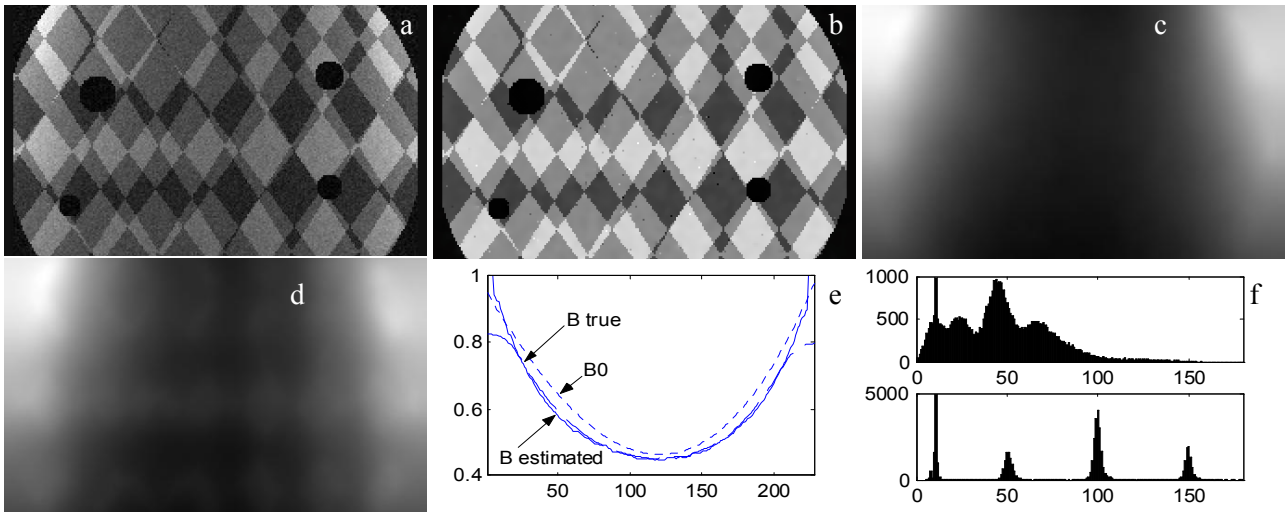

Figure 3. Panel (a) shows the original image of the digital phantom in the SNR=16 case and (b) the corrected image using the heavy filtering option. The corresponding bias estimated is (c). The panel (e) shows horizontal profiles of the initial (B_0), estimated (B) and ideal (B true) bias field. Histograms of original image (f top) and corrected (f bottom) illustrate the good performance of the method. The panel (d) displays the bias estimated using no pre-processing filtering where signal from the tissues are seen illustrating the sensitivity of the original AFCM method to the noise.

and (see [6] for details):

$$\nabla E_{b1} = \frac{\partial E_{b1}}{\partial b_j} = 2H_1 \otimes b$$
$$\nabla E_{b2} = \frac{\partial E_{b2}}{\partial b_j} = 2H_2 \otimes b \tag{12}$$

We can write the explicit first order scheme to update the bias field at iteration $t+1$ from its values at iteration t:

$$b_j^{t+1} = b_j^t + dt.[\sum_{k=1}^{N_c} u_{jk}^p . v_k (y_j - b_j^t v_k) - \alpha H_1 \otimes b\big|_j - \beta H_2 \otimes b\big|_j] \tag{13}$$

The algorithm stops when the cluster centers do not change significantly.

2.4. Background and outlier class

Our assumption is that some classes should have constant intensity across the image. We seek to estimate a smooth bias field such that the clusters associated with those classes are statistically meaningful. When a voxel contains a mixture of pure tissue or a tissue not encompassed by the already identified clusters, its influence in the class center calculation (v) will bias the cluster parameters and displace it from its optimal location. Outliers are taken into account using a noise cluster technique borrowed from robust statistics [16]. They are modeled as a uniform class across the range of possible data intensity. Including the background, the formulation of the cost function changes to:

$$E_{FCM} = \sum_{j\in\Omega} \left(u_{jb}^p \left\| y_j - \mu_n \right\|^2 + \sum_{k=1}^{N_c} u_{jk}^p \left\| y_j - b_j v_k \right\|^2 + uo_j \delta^2 \right) \tag{14}$$

relaxing the constraint (7) on the class membership of the N_c good clusters to include the membership of the outlier class (uo): $uo_j = 1 - \sum_{k=1}^{N_c} u_{jk}$. The classification tends to estimate a bias field making the identified tissue classes as constant as possible across the image while rejecting the voxels that are too different (figure 2).

2.5 Initialization and parameters choice

Good initialization of the bias is critical for the proper performance of the algorithm. A first rough estimation of the bias is performed by fitting a polynomial function to the original data. It provides a bias field close to the final solution and

reduces dramatically the number of iterations necessary to converge. Moreover, it avoids exploring unnecessary areas of the parameter space, and this greatly reduces chance of being trapped in local minima.

We determined experimentally to include three main tissue classes to reflect the main tissues present in the neck (i.e. skeleton muscles, interstitial tissue, and low signal cartilages and bones). A fourth class is the background class as identified above and an extra fifth class models the outlier voxels. Prior to classification, we divide the image by its maximal value and multiply by 100. During the classification, a class is kept constant at 100 implicitly forcing the maximum value of the bias field to remain around unity, acting as a scaling factor.

The computation burden is also reduced since only N_c-*1* cluster centers need to be updated. If MR acquisition parameters are comparable (same scanner, similar coil positioning, same sequences), using this scheme leads to consistent inter-patients and inter-slices class centers and provides a normalization methods to compare image data. Figure 1 shows the different steps of the method on actual patient data.

2.6. Experimental application of the method

We constructed a 256x256 image with three classes (50, 100 and 150). An actual MR scan from a homogeneous phantom compatible with a neck size has been acquired to measure a real sensitivity field (B_{true}) and multiply the ideal multiclass image. Outside the simulated neck, voxel values corresponding to air are set to a low background value (20). Disks of background are added to simulate lumen with no signal using typical location and size of carotids. In experiment where noise is being added, the synthetic image is Fourier transformed, summed with a normally distributed noise and inverse Fourier transformed. We compute the mean error of the estimated bias with respect to the original inhomogeneity in the simulated lumen areas dilated by 5 voxels to include hypothetical vessel wall locations. To evaluate the performance of the classification, we compute a misclassification rate by dividing the number of misclassified voxels by the total number of voxels (excluding background voxels).

Sixteen patients with carotid stenosis documented by duplex ultrasound were recruited for the study. Informed consent was obtained from all subjects under a protocol approved by the institutional review board for human investigation. All MR scans were conducted on a 1.5 T system (Magnetom Sonata; Siemens, Erlangen, Germany) with a custom-built phased array coil. Dark blood images were obtained using ECG-triggered double inversion recovery (DIR) turbo spin echo sequences. Imaging parameters (TR/TE/TI/NSA/thickness/FOV) were as follows: T1W: 1R-R/7.1ms/500ms/2/3mm/ 13cm; PDW: 2R-R/7.1ms/600ms/2/3mm/13cm; T2W: 2R-R/68ms/ 600ms/2/3mm/13cm. Fat saturation was applied. The in plane resolution was $0.51\times0.51\text{mm}^2$. For carotid artery bias correction, the parameters of the algorithm are α=7e5, β=7e4, Δt=1e-6, p=2, δ=10.

3. RESULTS

3.1. Performance evaluation on synthetic dataset

Figure 3 shows result with moderate noise of the bias estimate on synthetic phantom. The bias is correctly identified and the classification is successful.

Left graph in figure 4 shows for different levels of noise (SNR with respect to the class 150) and filtering (no filtering, using $\sigma_{AD} = \sigma_n\sqrt{2}$ and $\sigma_{AD} = 2\sigma_n\sqrt{2}$) superior results using the pre-processing filtering step. In the extreme case of signal-to-noise ratio <7, the error due to the bias estimation is less than 4% with filtering and still in the acceptable range of 10% without filter. The pre-filtering dramatically reduces the misclassification rate as expected by introducing spatial correlation among voxels.

3.2. Application to patient images

Figure 5 shows data on three patients with side-by-side comparison of original and corrected images. All corrected images are displayed with the same windowing (0 to 130) allowing direct appreciation of vessel wall signal intensity. Corrected, images are free from visible shading artifact and skeletal muscles are isointense across the images. On those PDW scans, fibrous tissue are hyperintense to the close sternocleidomastoid muscle as shown by several groups and are better discerned once the images are corrected. Good results are achieved even in the presence of significant noise.

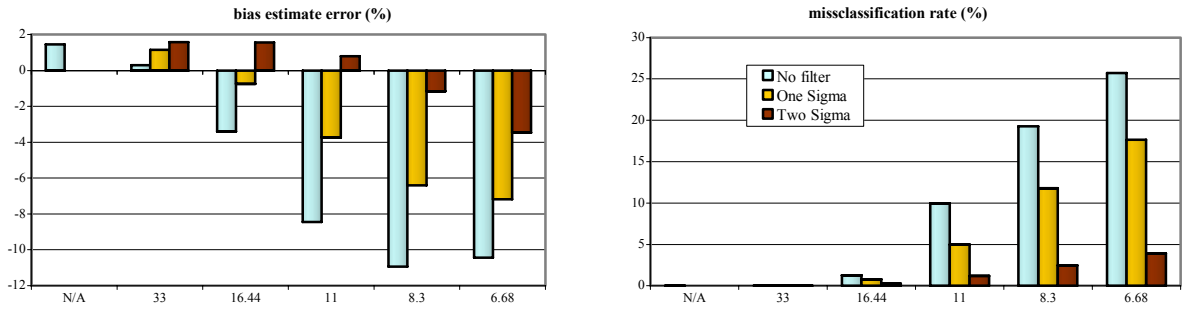

Figure 4. Left graph shows the variation error in percent of the bias estimate. Right graph reports the segmentation misclassification rate. Cases: no filtering, one sigma and two sigma filter illustrate the performance of the method. Abscise is the signal to noise ratio relative to the class 150.

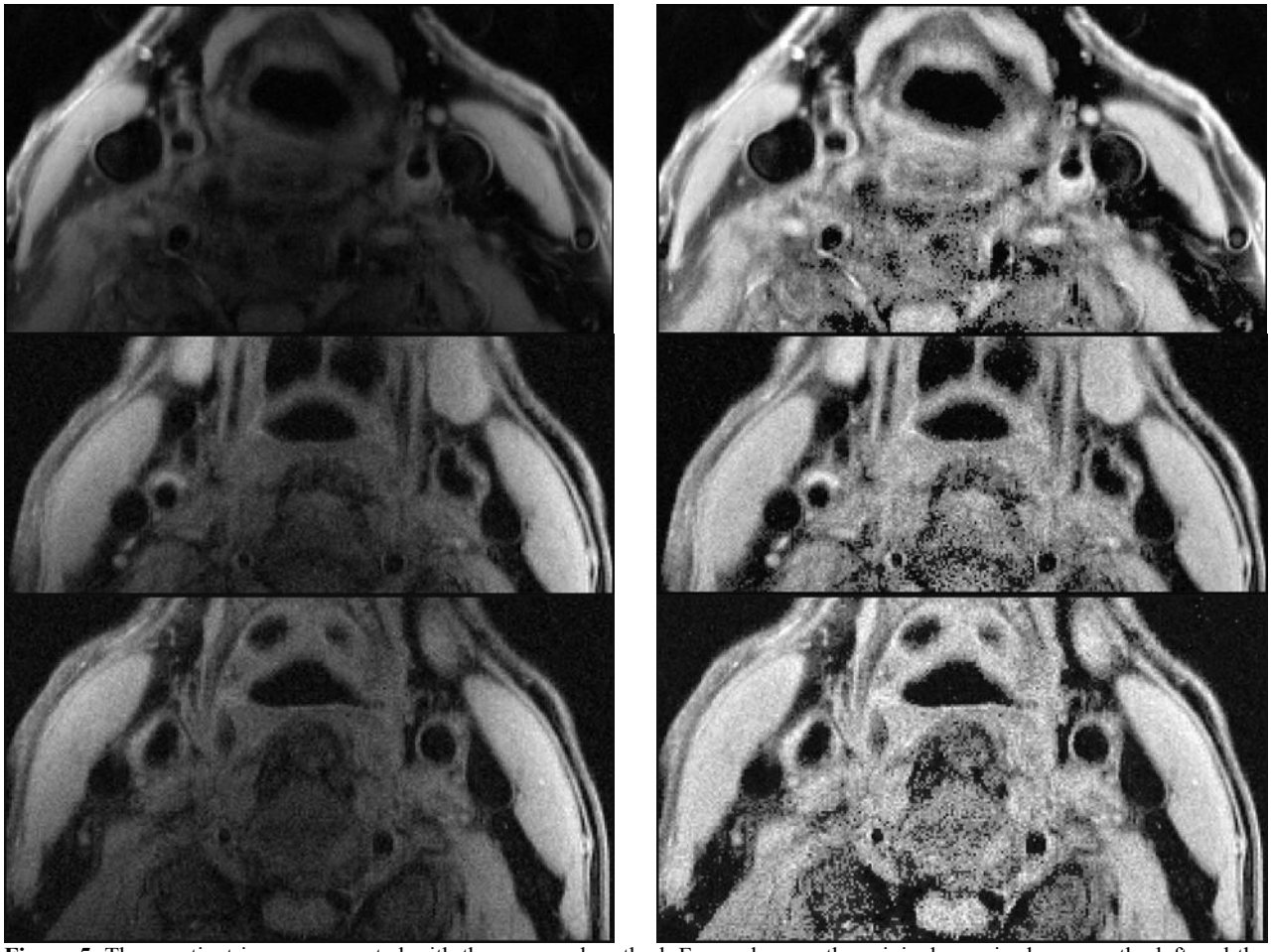

Figure 5. Three patient images corrected with the proposed method. For each case, the original scan is shown on the left and the corrected one on the right. All corrected images are displayed with the same windowing, while the original images are windowed individually for best display. Carotid arteries are zoomed in the inserts. The case on the right is particularly noisy. Note the easy comparison of vessel wall signal across patients after correction. Upper case is T1W, others are PDW.

4. CONCLUSION

Our method successfully corrects sensitivity inhomogeneity in MR images acquired with surface array coils for imaging the carotid arteries. The steep bias is corrected sufficiently to aid human interpretation of gray scales. It should also make possible computerized classification. Important modifications in the algorithm include automatic setting of anisotropic diffusion, free of bias field artifact, the automatic segmentation of background voxels to identify a background class and characterize additive noise, the initialization of the bias field to speed up the algorithm convergence, and a normalization technique for inter- and intra- patient data. Currently, we are working to test our method on a specially designed phantom.

REFERENCES

1 Quick,HH, Debatin,JF, Ladd,ME. MR imaging of the vessel wall. *European Radiology* 12:889-900.
2 Cai,JM, Hatsukami,TS, Ferguson,MS, Small,R, Polissar,NL, Yuan,C. Classification of Human Carotid Atherosclerotic Lesions With In Vivo Multicontrast Magnetic Resonance Imaging. *Circulation* 106:1368-1373.
3 Toussaint,JF, LaMuraglia,GM, Southern,JF, Fuster,V, Kantor,HL. Magnetic Resonance Images Lipid, Fibrous, Calcified, Hemorrhagic, and Thrombotic Components of Human Atherosclerosis In Vivo. *Circulation* 94:932-938.
4 Morrisett,J, ick,W, harma,R, awrie,G, eardon,M, zell,E, chwartz,J, unter,G, orenstein,D. Discrimination of components in atherosclerotic plaques from human carotid endarterectomy specimens by magnetic resonance imaging ex vivo. *Magnetic Resonance Imaging* 21:465-474.
5 Arnold,JB, Liow,JS, Schaper,KA, Stern,JJ, Sled,JG, Shattuck,DW, Worth,AJ, Cohen,MS, Leahy,RM, Mazziotta,JC, Rottenberg,DA. Qualitative and quantitative evaluation of six algorithms for correcting intensity nonuniformity effects. *Neuroimage* 13:931.
6 Pham,DL, Prince,JL. Adaptive fuzzy segmentation of magnetic resonance images. *Medical Imaging, IEEE Transactions on* 18:737-752.
7 Wells,WMI, Grimson,WEL, Kikinis,R, Jolesz,FA. Adaptive segmentation of MRI data. *Medical Imaging, IEEE Transactions on* 15:429-442.
8 Likar,B, Viergever,MA, Pernus,F. Retrospective correction of MR intensity inhomogeneity by information minimization. *Medical Imaging, IEEE Transactions on* 20:1398-1410.
9 Meyer,CR, Bland,PH, Pipe,J. Retrospective correction of intensity inhomogeneities in MRI. *Medical Imaging, IEEE Transactions on* 14:36-41.
10 Styner,M, Brechbuhler,C, Szckely,G, Gerig,G. Parametric estimate of intensity inhomogeneities applied to MRI. *Medical Imaging, IEEE Transactions on* 19:153-165.
11 Liew,AWC, Hong Yan. An adaptive spatial fuzzy clustering algorithm for 3-D MR image segmentation. *Medical Imaging, IEEE Transactions on* 22:1063-1075.
12 Haacke,EM, Brown R.W., Thompson M.R., Venkatesan R. *Magnetic resonance imaging - physical principles and sequence design*. 1999. Wiley-Liss, New York.
13 Black,MJ, Sapiro,G, Marimont,DH, Heeger,D. Robust anisotropic diffusion. *Image Processing, IEEE Transactions on* 7:421-432.
14 Lindeberg,T. Scale-space for discrete signals. *Pattern Analysis and Machine Intelligence, IEEE Transactions on* 12:234-254.
15 Bezdek JC, Hall LO, Clarke LP. Review of MR image segmentation techniques using pattern-recognition. *Med Phys* 20:1033.
16 Dave,RN, Krishnapuram,R. Robust clustering methods: a unified view. *Fuzzy Systems, IEEE Transactions on* 5:270-293.